NASA Langley's Approach to the Sandia's Structural Dynamics Challenge Problem

L.G. Horta, S.P. Kenny, L.G. Crespo, and K.B. Elliott

Abstract

The objective of this challenge is to develop a data-based probabilistic model of uncertainty to predict the behavior of subsystems (payloads) by themselves and while coupled to a primary (target) system. Although this type of analysis is routinely performed and representative of issues faced in real-world system design and integration, there are still several key technical challenges that must be addressed when analyzing uncertain interconnected systems. For example, one key technical challenge is related to the fact that there is limited data on target configurations. Moreover, it is typical to have multiple data sets from experiments conducted at the subsystem level, but often samples sizes are not sufficient to compute high confidence statistics. In this challenge problem additional constraints are placed as ground rules for the participants. One such rule is that mathematical models of the subsystem are limited to linear approximations of the nonlinear physics of the problem at hand. Also, participants are constrained to use these models and the multiple data sets to make predictions about the target system response under completely different input conditions.

Our approach involved initially the screening of several different methods. Three of the ones considered are presented herein. The first one is based on the transformation of the modal data to an orthogonal space where the mean and covariance of the data are matched by the model. The other two approaches worked solutions in physical space where the uncertain parameter set is made of masses, stiffnessess and damping coefficients; one matches confidence intervals of low order moments of the statistics via optimization while the second one uses a Kernel density estimation approach. The paper will touch on all the approaches, lessons learned, validation

metrics and their comparison, data quantity restriction, and assumptions/limitations of each approach.

Keywords: Probabilistic modeling, model validation, uncertainty quantification, kernel density

1. Introduction

To address the Sandia Challenge problem, NASA Langley assembled a group of researchers to study the tasking document and to interpret the information provided. Initially, after reviewing the documentation, it was apparent that no single approach appeared to be more suitable to tackle the challenge problem nor did a solution exist in the open literature. Instead, several different solution approaches were sought. In spite of the tremendous efforts of the Sandia group in crafting the challenge document, questions regarding the appropriateness of metrics, and what specifically were the "no modeling" ground rules still persisted and prompted many internal discussions. The two main modeling questions were: what was an acceptable level of modeling, and was the use of physical parameters, e.g., mass, stiffness, and damping for uncertainty modeling permitted. In the end, the work that is reported here maintains the spirit of the challenge problem, in our view, with Langley's interpretation of the Sandia task, which is provided explicitly later in the document.

From the onset it was clear that the key to obtaining a solution to the problem was to build probabilistic models for the parameters of the subsystem that could later be sampled in order to study the target system. Techniques to accomplish this would lead to models that "match" the experimental data provided. Without diminishing the work of statisticians, it was felt that a new solution approach would have to be tailored for this problem. Details on the proposed methods are presented next.

2. Problem Statement

In the interest of time, the reader is referred to the Sandia Challenge document in Ref. [1] for a detailed description of the problem formulation, goals, and objectives. However, because of the several possible interpretations of the document requirements, it is important to restate the requirements as interpreted by the Langley team. Rather than rephrasing our interpretation of the requirements, it is best to postulate a series of questions that this work will attempt to address: 1) Is a linear time invariant (LTI) representation of the 3-degrees-of-freedom (DOF) subsystem adequate to describe the nonlinear response data, i.e., does this simple model adequately capture the physics of the problem? 2) What metric(s) properly quantifies the agreement between a subsystem model and the experimental data? 3) How are the metrics computed and what are the associated confidence levels? 4) What are the acceptance/rejection criteria of the model and is the model found to be adequate by the criteria? 5) How can one determine that a model based on calibration data is suitable for validation? 6) Is updating of the calibration model recommended before using it to evaluate the accreditation data, and if so what is the updating process? 7) What is the impact of having additional number of tests in the database? How is this benefit/impact quantified?

Answering each of these questions in a comprehensive manner is impossible in the time allotted to work this problem. Nonetheless it is recognized that the main purpose of the challenge is to address each question. Consequently, as a compromise, each solution approach was evaluated on its ability to address each question. Many approaches were abandoned due to their inability to answer a particular aspect of the problem.

As a final note, it is important for the reader to remember that the same definitions in the Sandia document are used in the paper. For example, the subsystem is a 3 mass/spring/damper system with inputs applied at mass 1 for the calibration data and mass 2 for the validation data.

This subsystem is referred to as the 3 degrees-of-freedom linear time invariant 3-DOF LTI. When this 3-DOF LTI system is attached onto a flexible beam, it is referred to as the accreditation system but when attached onto a higher fidelity beam model it is the referred to as the target system.

3. Evaluation of the LTI Model Scripts Using Metrics

In this section, the adequacy of the LTI representation of the 3-DOF subsystem is studied. Unlike problems where engineers start with the physics, formulate the problem, and then solve it, for the challenge problem a set of MATLAB scripts were provided to approximate the physics of the 3-DOF nonlinear system. The goal here is to assess the adequacy of the scripts with respect to the nonlinear response data. For this, a metric that depends on the approximated lower and upper bounds of the support of the maximum and minimum singular values was used. If H_M is the Frequency Response Function (FRF) matrix of the model and H_T is the one extracted from the experimental data, model adequacy requires

$$\underset{\forall d_l}{Max}\ \bar{\sigma}(H_M(j\omega, d_l)) \geq \underset{\forall d_i}{Max}\ \bar{\sigma}(H_T(j\omega, d_i)) \tag{3.1.1}$$

and

$$\underset{\forall d_l}{Min}\ \underline{\sigma}(H_M(j\omega, d_l)) \leq \underset{\forall d_i}{Min}\ \underline{\sigma}(H_T(j\omega, d_i)) \tag{3.1.2}$$

where d_l is the vector of uncertain parameters, ω is the frequency, $\bar{\sigma}$ is the maximum singular value of the input-output matrix, and $\underline{\sigma}$ is the minimum singular value. This metric will be used to evaluate the script for the 3-DOF LTI model provided.

Although 60 calibration data sets were provided only 20 are statistically independent. For each experiment, the corresponding parameter data set was used with the script, i.e. H_M, to simulate the 3-DOF system response and to compute Eqs.(3.1.1)-(3.1.2). Figure 1.a. shows with a solid blue line the test data and with a dotted red line are results using the Sandia script for the calibration experiments. $\bar{\sigma}$ for test and model are the top two lines and $\underline{\sigma}$ are the bottom two lines. Discrepancies in the lower singular value bound prompted a close examination of the

Sandia scripts that revealed numerical problems with a matrix inversion operation. After replacing a numerical matrix inversion with its closed-form solution, the curves in Fig. 1.b. were computed.

Despite the fact that results with the modified script proved to be better, when comparing singular values, it is still difficult to judge how well the 3-DOF LTI model predicts time observations. For this another metric was defined in terms of the 95% confidence intervals of the mean value of the maximum acceleration. Because of the limited number of experimental data sets, a *t*-distribution was used to determine confidence intervals for both test and analysis. For adequacy assessments, whenever possible the number of data sets for test and analysis was kept the same. This metric is given by the bounds of the 95% confidence intervals of the maximum acceleration based on the *t*-distribution. This implies that

$$P\left[\overline{a} - t\,S/\sqrt{n} < a < \overline{a} + t\,S/\sqrt{n}\right] = 0.95 \tag{3.1.3}$$

where $\overline{a}$ is the mean of the maximum acceleration, t is the *t*-distribution scaling for a population size of n, and S is the sampled standard deviation. We use this metric to compare the models corresponding to the Sandia script and the modified script. Figure 2a shows the mean of the maximum acceleration from test on the abscissa and results for the original Sandia script along the ordinate for subsystem masses 1, 2, and 3, as labeled. Superimposed at each estimated mean value are the 95 % confidence intervals plotted as thin bars for both test and the script; horizontal bars for tests and vertical bars for analysis. Data points for the mean of the maximum acceleration on the diagonal line indicate exact matching between the test and the model. Same information for the modified script is shown in Figs. 2a and 2b. To contrast this with results shown earlier, the Sandia and the modified scripts yield similar results. Consequently, the need to use different metrics to assess adequacy of LTI models even in those cases where the model

predicts well a particular observation is extremely important. Hereafter, the modified script will only be used.

4. Definition of Metrics Used for Evaluation

In the Sandia challenge document, a certification metric was provided to assess the survivability of a subsystem under loads and uncertainty. However, to evaluate the matching between the experimental data and the subsystem model two additional metrics have been chosen; a frequency domain metric using singular values of the FRF similar to those used in Refs. [2]-[3], and one that compares maximum acceleration and the corresponding confidence intervals. To define Metric 1, let $\sigma(H)$ be a diagonal matrix of singular values of the FRF. The average singular value over *n* observations is

$$\text{Metric } 1 = \frac{1}{n}\sum_{l=1}^{n} tr\left(\sigma(H(j\omega, d_l))\right) \tag{4.1.1}$$

where *tr*(·) is the trace operator. This metric is computed not only for the model's FRF, $H_M(j\omega, d_l)$ but also for the test $H_T(j\omega, d_l)$. Since the singular values of the FRF's are random processes dependent on the frequency, several of their moments can be calculated and used for comparison to ascertain model "correctness". Another important aspect of this metric is the fact it is independent of the input form, e.g., broadband, short pulse, sinusoidal, etc. Consequently, it is focused on the LTI structure and the numerical solution approach and not on how a particular input propagates through the model.

Although the singular value metric works well to study matching in frequency domain, it is also important to establish a time domain metric to get a more direct look at the certification criteria. For this, the metric introduced in Section 3, referred hereafter as Metric 2, will be used. Hence, Metric 2 is given by the bounds of the 95% confidence intervals of the maximum acceleration. Hence,

$$\text{Metric } 2 = \left[\bar{a} - t\,S/\sqrt{n}, \bar{a} + t\,S/\sqrt{n} \right] \tag{4.1.2}$$

5. Probabilistic Modeling

In the following sections three probabilistic modeling methods are presented to create new parameter populations from experimental data observations. These are the methods used to address the certification problem later in the paper.

5.1. Probabilistic Modeling Approach (PM-1)

Although there are many aspects of the challenge problem that have to be carefully addressed, the most important aspect is the approach used to generate parameter values outside the given data set. Any solution approach must not only provide parameter data values beyond what was provided but more importantly these new parameter values should exhibit similar statistics. Although matching of the statistical features is a reasonable approach to follow, there are many dimensions of the matching process that could be examined. In this approach, the mean and covariance of the modal data are matched by a correlated normal random vector. This approach transforms the data from the parameter space to an orthogonal space using singular value decomposition. It is in this orthogonal space that a normal distribution is built. The correlation in the data is captured by designing the filter Γ. The steps to design the filter are explained next.

First, the three data sets for high, medium, and low inputs are averaged in order to obtain an independent sample. To avoid numerical conditioning problems that often arise when parameters have drastically different magnitudes, the data are then normalized using the maximum value of the parameters. The normalized data will be referred to as the parameter matrix *D,* where $D = [d_1 \quad d_2 \quad \cdots \quad d_n]$. The next step is to decompose the parameter matrix into principal components using singular value decomposition (SVD). Given a $k \times n$ parameter

matrix assembled from n observations of k parameters in the vector d, its SVD decomposition is written as;

$$\underbrace{D}_{k\times n} = \underbrace{U}_{k\times k}\ \underbrace{S}_{k\times n}\ \underbrace{V^T}_{n\times n} = U[s \quad 0]\begin{Bmatrix}\eta\\ \delta\end{Bmatrix} = U\ \underbrace{s}_{k\times k}\ \underbrace{\eta}_{k\times n} \tag{5.1.1}$$

Since the number of observations n is greater than the number of parameters k, there are only k nonzero singular values in the matrix S and they are stored in the matrix partition s. Furthermore, Eq.(5.1.1) shows the partitioning of V to separate those columns associated with the nonzero singular values. Since the vectors in U form a k^{th} dimensional orthogonal set, by using the transformation $T \triangleq Us$ the problem can be transformed from the input parameter space d to an orthonormal space η using $\eta_j = T^{-1}d_j$, where η_j is the j^{th} column of η. In this transformed space it is possible to truncate the parameter space according to the singular value magnitudes. Although truncation is not performed in PM-1, both PM-2 and PM-3 employ reduced dimension uncertainty models.

To generate a new population to approximate the random vectors in the columns of the transformed space η, define a new $k\times 1$ random vector $n_e = \Gamma\gamma$ where γ is a $k\times 1$ random vector from a normal distribution with $E[\gamma] = \Gamma^{-1}\mu$, $E[\gamma\gamma^T] = I$, and Γ is a filter matrix yet to be defined. In this definition μ is the expected value of the transformed parameter vector $\mu = E[\eta_j]$ and the data covariance in the transformed space is $Q = E[\eta_j\eta_j{}^T] = \Gamma\Gamma^T$. This last equality is a result of a Cholesky decomposition of the data covariance matrix. Hence, using these definitions $E[n_e] = \mu$, $E[n_e n_e^T] = Q$, and $E[d] = T\mu$. This process is similar to that of defining a fully correlated multi-variable normal distribution, but the added flexibility is in the ability to truncate the parameter space using singular values.

5.2. Probabilistic Modeling Approach (PM-2)

This approach consists of two main steps, namely, the uncertain space truncation and the sizing of a joint Probability Density Function (PDF). In the former step, the dimension of the uncertain parameter space is reduced by approximating the dependencies among the uncertain parameters with linear combinations. This step is based on the SVD of the matrix of observations. Joint PDF sizing is carried out in the resulting space, by solving an optimization problem that minimizes the offset, to be defined later, between the observations and the predictions for the subsystem. Inequality constraints are used to prevent identifying models leading to infeasible subsystems. Details on the implementation of these steps are presented next.

5.2.1. Truncation of the Uncertain Parameter Space

In contrast to PM-1, which works with modal parameters directly, this approach uses physical parameters. Consequently, the row dimension of the parameter matrix is k=9 and not k=15 as presented in PM-1. The approach developed here will define the uncertainty space as a general r-dimensional space, with specific numerical values for r given later in the paper. As before, the high-, medium- and low-level excitation results for the same realization of the subsystem are first averaged to make a statistically independent sample. In contrast to the PM-1, this method normalizes the data using the estimated mean value of the parameters. The normalized data will be collected in the observation matrix X. As a result, the i^{th} row vector of X_{ij} contains the mean-normalized observations of the i^{th} parameter. The SVD of this matrix leads to

$$\underset{k\times n}{\underbrace{X}} = \underset{k\times k}{\underbrace{U}}\ \underset{k\times n}{\underbrace{S}}\ \underset{n\times n}{\underbrace{V}} \tag{5.1.2}$$

An r-dimensional approximation to this matrix is given by

$$\underset{k\times n}{\underbrace{\widehat{X}}} = \underset{k\times r}{\underbrace{U}}\ \underset{r\times r}{\underbrace{S}}\ \underset{r\times n}{\underbrace{V}} \tag{5.1.3}$$

where the underlined matrices result from extracting sub-matrices from Eq. (5.1.2) in the referred positions, e.g. $\underline{U}$ has the same first r columns of U. This approximation is equivalent to setting the smallest non-zero k-r singular values of the matrix S in Eq.(5.1.2) equal to zero. The approximation error due to truncation, given by

$$e(r) = \sum_{i=1}^{k} \sum_{j=1}^{n} \left(\widehat{X}_{ij} - X_{ij} \right)^2 \tag{5.1.4}$$

is used in the truncation process to select r.

Note that Eq. (5.1.3) contains a linear combination of r uncorrelated parameters (the ones in V), possibly dependent among themselves, that approximates the k parameters of interest (the ones in X). Hereafter, we will refer to the k parameters in the left hand side of Eq.(5.1.2) as the *Target Parameters* and to the r parameters of $\underline{V}$ in Eq. (5.1.3) as the *Slack Parameters*. While the target parameters might have a clear physical interpretation, e.g. they could be in either the modal or the physical space, the slack parameters do not.

If an r-dimensional probabilistic model of the slack parameters is available Eq.(5.1.3) can be used to generate samples of the target parameters. The resulting subsystem model however, must be able to prevent the occurrence of infeasible subsystem realizations. This requirement is achieved by parameterizing the slack parameters in terms of r target parameters. Such a step will be referred to as the re-parametrization. Its implementation is as follows. From Eq. (5.1.3) select an arbitrary set of r row equations out of the k available. This set can be written as

$$\underset{\sim}{\underset{r\times n}{B}} = \underset{\sim}{\underset{r\times r}{C}} \; \underset{\sim}{\underset{r\times r}{S}} \; \underset{\sim}{\underset{r\times n}{V}} \tag{5.1.5}$$

where B is extracted from $\widehat{X}$ and C is extracted from $\underline{U}$ and $\underline{S}$. If C is a non-singular matrix Eq.(5.1.5) provides the desired re-parameterization. Combining Eqs. (5.1.2) and (5.1.5) one can obtain the approximation

$$\underbrace{\hat{X}}_{k\times n} = \underbrace{\underline{U}}_{r\times r}\underbrace{C^{-1}}_{r\times r}\underbrace{B}_{r\times n} \tag{5.1.6}$$

This expression provides a parameterization of the k target parameters in terms of an r-dimensional subset. Since the r parameters in B have a clear physical interpretation, one can easily construct a sound probabilistic model for them.

Once r rows of $\hat{X}$ are selected to form B, the independent parameters in Eq.(5.1.6) are prescribed. If such parameters are not a basis for the corresponding space, approximation error is introduced. In practice, this error will always be present. In order to minimize such an error, we select the combination of r target parameters that makes the condition number of C as close as possible to one. The closer the condition number is to one the smaller the approximation error.

5.2.2. Joint PDF Sizing

Equation (5.1.2) and a n-dimensional probabilistic model of uncertainty for the parameters in V, constitute one type of uncertainty model for the subsystem paramters. Similarly, Eq. (5.1.3) and a r-dimensional probabilistic model of uncertainty for $\underline{V}$ constitute another type, one for which truncation error is present. Another type results from using Eq. (5.1.6) and a r-dimensional probabilistic model of uncertainty for B. The resulting model for this type has both truncation and re-parameterization error.

In this section we will consider the model based in Eq. (5.1.6). Hence, the only task that remains to be done is to determine a r-dimensional joint PDF for the uncorrelated, possibly dependent, parameters in B. Assume that a sample of the r parameters in B, namely b, is given by

$$b = \underbrace{\underline{A}}_{r\times r} h(q) \tag{5.1.7}$$

where A is a transformation matrix, and $h(q)$ is a sample of an r-dimensional vector of independent random variables. The vector q is used to explicitly refer to the parameters that

specify the PDF of h while the matrix A is used to allow for correlation of the independent variables. However, the free parameters A, q and the structure of h are to be specified.

If the target parameters are physical parameters, the components of b must be strictly positive. This requirement is attained by selecting a matrix A whose components are non-negative, and by choosing a PDF for h whose support can only assume non-negative values.

Once the structure of h is prescribed, e.g. h is lognormal, we have r^2 unknowns and r^2 constraints from A, and $dim(q)$ unknowns from h. In what follows, we assume that h is a vector of independent lognormal random variables. Hence, $dim(q)=2r$.

If Eq. (5.1.6) is rearranged such that the first r target parameters in $\hat{X}$ are the ones in B; joint PDF sizing is performed by solving the following optimization problem

$$< A, q >= \operatorname{argmin}\{p^{\mathrm{T}} W p : A_{ij} > 0 \text{ for } i = 1,...,r \text{ and } j = 1,...,r \\ U' C^{-1} A_{ij} \geq 0 \text{ for } i = r+1,...,k \text{ and } j = 1,...r\} \tag{5.1.8}$$

where p is a vector composed of metrics that quantify the offset (to be introduced later) between the observations and the predictions of the model, and W is an arbitrary, strictly positive, weighting matrix. The constraints in Eq. (5.1.8) are solely used to eliminate models leading to physically unrealizable subsystems.

There are many ways to quantify the "offset" in p. The metrics considered are introduced next. In what follows we will denote by x_0 the r-dimensional vector of target parameters in B corresponding to the observations and by x_m the one corresponding to the model. Note only r target parameters are used to size the joint PDF.

5.2.3. Low Order Statistics

Arbitrary order statistical moments of the target parameters can be readily approximated from the observations. However, since the population size is quite small, only the first few moments

are meaningful. For this reason we have only considered the first, second and third order moments of the target parameters. On the other hand, the predicted moments resulting from using Eqs.(5.1.6)-(5.1.8) and any given q, can be calculated analytically. Details on their calculation are omitted due to space limitations. The metric of interest is

$$offset_1 = w_1^T \begin{bmatrix} \|Q[x_0]-E[x_M]\| \\ \|Q[x_0 x_0^T]-E[x_M x_M^T]\| \\ \sum_{j=1}^{r} \|Q[x_{0j} x_0^T x_0]-E[x_{Mj} x_M^T x_M]\| \end{bmatrix} \tag{5.1.9}$$

where $w_1 \geq 0$ is a vector of weights, Q[·] is the sampled-mean operator, E[·] is the expected value operator, and ||·|| is the Euclidean norm. Note that this offset does not take into account the population size, e.g. the fact that for the calibration experiment there are only n=20 statically independent observations available.

5.2.4. Confidence Intervals of the Low Order Statistics

This metric quantifies the offset between the 95% confidence intervals of the statistics in Eq.(5.1.9). To implement this, n (the same number of observations available) Hammersley Sequence samples (HSS) [4] of the subsystem model are generated. This sampling method is used since the resulting samples not only characterize well the joint PDF but also because they are deterministic. Note that these confidence intervals measure the sampling PDF of the statistics, which is assumed to be Gaussian. The Maximum Likelihood Estimator method (MLE) is used to calculate these intervals.

If the 95% confidence interval of the random variable a is denoted as $[\gamma^-(a), \gamma^+(a)]$, the corresponding metric for this offset is

$$offset_2 = w_2{}^T \begin{bmatrix} \|\gamma^-(Q[x_0])-\gamma^-(Q[x_M])\|+\|\gamma^+(Q[x_0])-\gamma^+(Q[x_M])\| \\ \|\gamma^-(Q[x_0x_0{}^T])-\gamma^-(Q[x_Mx_M{}^T])\|+\|\gamma^+(Q[x_0x_0{}^T])-\gamma^+(Q[x_Mx_M{}^T])\| \\ \sum_{j=1}^{r} \| \|\gamma^-(Q[x_{0j}x_0x_0{}^T])-\gamma^-(Q[x_{Mj}x_Mx_M{}^T])\|+\|\gamma^+(Q[x_{0j}x_0x_0{}^T])-\gamma^+(Q[x_{Mj}x_Mx_M{}^T])\| \end{bmatrix} \quad (5.1.10)$$

where $w_2 \geq 0$ is a vector of weights. If more observations are available, smaller confidence intervals for the statistics result. This will reduce the freedom available for sizing the joint PDF that exist when n is small, i.e. the offsets corresponding to different subsystem's models differ more as the number of observations increases.

5.3. Probabilistic Modeling Approach 3 (PM-3)

Kernel Density Estimation (KDE) provides another technique to approximate unknown parameter distributions functions from observations. Due to space limitations, the technical details of the KDE approach, found in Ref. [6], will not be discussed here. Instead, potential users are referred to the MATLAB-based program called the Kernel Density Estimation Toolbox described in Ref. [7], which is a Multivariate KDE software package that was utilized in this paper. The general appeal of the KDE approach is that it does not impose a parametric form on the density function estimate prior to any actual estimation.

Similar to PM-2, this approach operates on data in the physical domain (mass, stiffness and damping) as opposed to the modal domain (frequency, modal damping, and mode shapes) as in Probabilistic Model 1 (PM-1). Furthermore, analogous to PM-2, the KDE approach in PM-3 will employ the singular value decomposition presented in Eqs.(5.1.2) and (5.1.3) to reduce the dimensionality of the uncertainty space. For this, the error metric in Eq.(5.1.4) is also used to control truncation error when selecting r in Eq. (5.1.3). Again, as in PM-2, avoidance of non-physical parameter values must be guaranteed. In PM-3, this is achieved using a brute-force method of sampling the identified kernel density estimates using very large sample sets and

rejecting those density estimates that produced non-physical values. There has been a great deal of research on kernel density estimation and it is well-known that the selection of the actual basis functions is not as critical as is the selection of the basis function's bandwidth, see Ref. [6]. Nonetheless, the KDE Toolbox does provide user-selectable basis functions as well as a variety of methods to prescribe their bandwidths. The results obtained in this work use Gaussian basis functions with bandwidths computed using the plug-in approach, see Ref. [7] toolbox, for minimizing an approximate mean integrated square error criterion.

The steps used in generating the kernel density estimates area as follows:

1. The raw modal data is processed to provide physical parameters (M, C, and K). This is done separately for both calibration and validation data sets for all force levels.
2. Physical data for the three force levels is averaged to provide one parameter set for each of the twenty system realizations, resulting in twenty data sets using calibration data and twenty data sets using validation data.
3. Singular value decomposition can be performed on the aggregate [M,C,K] combined dataset generated in step 2, or separately for [M], [C], and [K]. Regardless, the dimension of the uncertainty space is selected using the error in Eq. (5.1.4). Note that the data for step 2 may be treated separately, i.e., two sets of twenty points, one for calibration and one for validation, or as a single forty point dataset (calibration and validation combined). Both approaches are used.

Once the data had been properly processed, the KDE is performed as outline above.

6. Probabilistic Modeling Results

In the following, results from the PM-1, PM-2, and PM-3 approaches are used to predict the behavior of the accreditation and target system, but first results from each approach with the

subsystem only are discussed. Also discussed is the evaluation of the certification criterion by sampling the resulting subsystem models.

6.1. Probabilistic Method-1 (PM-1)

Recall that this approach matches mean and variances of the experimental data. To give an idea of the type of matching achievable with this approach, Fig. 3a shows six plots, top three leftmost show mode 1, 2, and 3 frequencies, and bottom three are the corresponding damping values. Star symbols correspond to calibration and validation data while superimposed are lines for the 99.9% confidence intervals obtained using a maximum likelihood estimate. Figure 3b shows the experimental covariance matrix $E[\eta_j \eta_j^T]$ in transformed coordinate space at the top and the computed covariance using 40 data sets at the bottom. As expected, the computed covariance matrix does not match exactly that of the experimental data set for small sample sets. In order for the two to agree, an infinite number of samples would be required.

A better way to evaluate a PM approach is to sample the resulting subsystem model and to evaluate the sample mean and representative percentiles of Metric 1.Fig. 4 shows these results for a parameter population of 200 samples. In here, the solid blue line is the experimental average from 20 calibration data sets whereas in dashed red is the sampled mean of the model and dashed greens are the corresponding 5 and 95 percentiles, i.e. if F denotes a sampling-based approximation to the Cumulative Distribution Function (CDF) of the random process associated with the singular values, the percentiles $l_1(\omega)$ and $l_2(\omega)$ are curves satisfying $F(l_1) = 0.05$ and $F(l_2) = 0.95$. Similarly Fig. 4b, shows results for the combined 20 calibration and 20 validation data sets; solid blue is the averaged for the experiments, dashed red is the model mean, and dashed green are the 5 and 95 percentiles. A subtle difference in the computation from Fig. 4a and 4b worth mentioning is the fact that in Fig. 4b, the singular value metric contains data from

two different inputs. A quick view of the plots shows that PM-1 and the 3-DOF LTI model predicts the average experimental results very well and that the percentiles are able to explain observations even in the presence of significant variations in the experimental response.

6.2. Probabilistic Method-2 (PM-2)

The approach presented in Section 5.2 was applied to the structural dynamics challenge, and the main observations and results are presented next. Since the structure of the subsystem is known, working in the physical parameter space allows one to reduce the dimension of the uncertain parameter space from 12 to 9, i.e. from ω_i, ζ_i and ϕ_i for i=1,2,3 with the three mass normalized equality constraints for the eigenvectors, to m_i, k_i and c_i for i=1,2,3. The truncation error of Eq. (5.1.4)for the calibration and validation data and the random vibration experiments led us to chose r=4. At such value, e=0.0426 and the best set for re-parameterization is given by m_2, c_2, k_1 and k_3.

Several joint PDFs were sized using different Ws in Eq.(5.1.8). Due to space limitations, we only present here results corresponding to one for which the offset metrics in Eqs.(5.1.9) and (5.1.10) were combined.

In the figures that follow, information for all target parameters is displayed even tough the sizing of the joint PDF was performed using only four of them. In other words, while Eq. (5.1.8) only uses information on m_2, c_2, k_1 and k_3, the figures show statistics and confidence intervals corresponding to the 9 physical parameters. Calibration and the validation data were used to generate PM-2. Figure (5) shows the low order statistics for the observations (line with dots) and the model (line with circles). A small offset between the observations and the model is attained. Figure (6) shows the confidence intervals for the standard deviation of the statistics in Figure (5) using the same line convention. A good matching of the confidence intervals was also attained.

Note that a good matching in the sense of Eq.(5.1.9) does not imply the one of (5.1.10), and vice versa.

As with PM-1, PM-2 is now compared to the experimental data using Metric 1. Figure 7a shows Metric 1 for calibration data and calibration/validation in shown in 7b for a parameter population of 200. As before, the solid blue line corresponds to the mean of the experimental data, dashed red is the model mean, and dashed green lines are the 5 and 95 percentiles. Similar to results shown in Fig. 4, the average from experiments is predicted well by PM-2 and the percentiles indicate that this model would also capture significant off-nominal experimental observations.

6.3. Probabilistic Method 3 (PM-3)

The KDE method, as presented in Section 5.3, was used to model the uncertain 3-DOF LTI subsystem data. The approach taken was to develop a KDE model for each of the physical parameters independently, i.e., treat [M], [C], and [K] separately. Employing Eq. (5.1.4) to determine the effect of truncation error results in a one-dimensional subspace for K and two-dimensional subspaces for M and C, i.e, $[r_k, r_m, r_c]=[1,2,2]$, for a total of five parameters. Comparisons of the normalized identified KDE models parameters versus those from the calibration data are shown in Fig. 8, with differences less than one percent.

As before, the PM-3 model is evaluated using Metric 1. Figure 9 shows the corresponding results using the same convention of Figs. 4 and 7 for the calibration data. It is seen that the mean of KDE model tracks test mean (in blue) well, but more importantly stays within the percentiles throughout the frequency range of interest.

7. Discussion of results for target and accreditation system

Until now the discussion focused on the 3-DOF LTI subsystem model and the development of probabilistic models for the parameters. However, it is important to remember that the goal of

the challenge problem is to make predictions, using what was learned from the subsystem to predict failures when integrated into the accreditation and the target system. Assessments for this, based on PM-1, PM-2, and PM-3 are presented next

To begin studying the accreditation system, adequacy of the integrated model provided by Sandia must be addressed first, where the model now includes the 3-DOF LTI, PM-1, or PM-2, or PM-3, and a model of a flexible beam. Due to space limitations, the results in the following are from probabilistic models obtained using the calibration data only, but results with both calibration and validation are comparable. Figure 10a and b shows results for Metric 1 and 2, respectively, using PM-1 with a parameter population arbitrarily chosen to be 200. Results for Metric 1 are shown in Fig. 10a with the solid blue lines corresponding to data from three experiments, whereas dashed lines correspond to the mean (red) and the 5 and 95 percentiles for the model. It is reasonable to assume that if the model is to fully explain the test observations all test results must lie within the arbitrarily selected percentiles bounds. This is the case for most of the frequency points. To contrast, time domain results for Metric 2 are shown in Fig. 10b with the abscissa showing the mean of the maximum acceleration for test versus model results plotted along the ordinate. To show uncertainty, lines from the mean, labeled 'o', shows the 95 % *t*-distribution confidence interval of the mean; horizontal lines for test and vertical lines for analysis. Since the analysis results are obtained with a population of 200, the uncertainty bounds are significantly smaller than test, which only has 3 data sets. Also note that the results for maximum acceleration of Mass 3 are close to the diagonal, indicating excellent matching of mean value predictions with tests.

Results for Metrics 1 and 2 using PM-2 and PM-3 approaches are shown in Figs. 11 and 12. Amazingly, in spite of the drastically different approaches, when compared through the output of

the accreditation system the same conclusions can be drawn as for PM-1. However, both PM-2 and PM-3 are able to realize a parameter population using a 4^{th} and a 5^{th} dimensional probabilistic model as opposed to 15 in PM-1, hence, significantly reducing the dimensionality of the uncertainty space.

Finally, to investigate survivability of the subsystem as part of the target system, PM-1, PM-2, and PM-3 are all used along with a prescribed excitation signal to compute the failure probability as stated in the Sandia document:

$$P_f = P[\max|a_3(t)| > 1.8 \times 10^4 in/\sec^2] \qquad (7.1.1)$$

The CDF of the maximum absolute value of the acceleration of mass three will be used to evaluate the models from calibration, validation, and accreditation data and to make a prediction on the target system response. Results for the case using Calibration data only are shown in Figure 13 in terms of the CDF for PM-1 in 13a, PM-2 in 13b, and PM-3 in 13c. With all three methods a parameter population of 5000 is used and outputs are generated for each case. As noted in the figure the failure probabilities predicted with PM-1 is 0.17, PM-2 is 0.22, and PM-3 is 0.20. But no significant difference in the shape of the CDF nor the in support set of the random variable is noticeable. Consequently, when the probability values are compared to the accreditation requirement that $P_f < 10^{-2}$, all three methods predict failure of the subsystem on the target system. Figure 14 shows the CDF results for the case when both calibration and validation data are used. In contrast to the results in Fig. 13, the failure probabilities predicted with PM-1 is 0.13, PM-2 is 0.12, and PM-3 is 0.20. Although slightly different from the case with calibration data only, this case also predicts failure of the subsystem. Also noticeable is how similar the CDF are among themselves and as compared to the ones in Fig. 13 and 14.

However, the failure probability estimate corresponding to PM-1 and PM-2 are considerably more sensitive to the inclusion of the validation data than the one from PM-3.

8. Concluding Remarks

Three approaches to parameter uncertainty modeling, based on experimental data, have been proposed and applied to the Sandia Challenge problem. To assess the adequacy of the model structure in the Sandia scripts and our ability to predict experimental observations, two metrics were defined and used to validate models at the subsystem and system levels. When using a frequency response metric a numerical deficiency of the Sandia script surfaced, but later it proved not to significantly impact the maximum acceleration. Note however, that this single metric does not imply a good matching in the time-domain per se. Amazingly, all three approaches produced almost identical CDFs for the acceleration performance metric and consistently showed that the regulatory requirement for the target system was violated. Nonetheless, using PM-2 and PM-3 the number of parameters needed to describe the uncertainty was reduced from 15 to 4 and 5.

For this particular problem, all three probabilistic methods, created using calibration data only, provided consistent results and predicted failure of the target system. The inclusion of the validation data did not substantially change the assessments resulting from using calibration data only. Finally, the fact that all three methods produced similar results is only an indication that data quantity limitations did not allow for the proper exploitation of strengths and weaknesses of each technique. Clearly, PM-2 and PM-3 reduction in the number of parameters required to fully characterize the uncertainty is remarkable.

9. Acknowledgements

The authors would like to thank Dr. J-S Lew for his work using interval analysis to address the challenge problem and to Dr. K.B. Lim for initial discussions while seeking solution approaches.

10. References

[1] Red-Horse, J.R., Paez, T.L.: "Sandia National Laboratories Validation Workshop: Structural Dynamics Application," *Validation Methodology Workshop at Sandia National Laboratories*, May 22-23, 2006.

[2] Horta, L.G., Reaves, M.C., Lew, J.-S.: "A Procedure for Static and Dynamic Model Update of Finite Element Models: Application to an Inflated/Rigidized Torus." Proceedings of the IMAC XXIV: Conference and Exposition on Structural Dynamics, 2006, St. Louis Missouri

[3] Hasselman T., Yap K., Yan H. and Parret, A.: "Statistical Energy Analysis by Principal Components for Mid-Frequency Analysis." Proceedings of the 43rd AIAA/ASME/ASCE/AHS/ASC Structures, Structural Dynamics, and Materials Conference, April 2002, Denver, CO. AIAA 2002-1395

[4][Robinson, D, Atcitty, C.: "Comparison of Quasi and Pseudo-Monte Carlo Sampling for Reliability and Uncertainty Analysis," AIAA-99-1589

[5] Silverman, B. W., Density Estimation for Statistics and Data Analysis, Chapman and Hall, New York 1986.

[6] Ihler, A., Inference in Sensor Networks: Graphical Models and Particle Methods, Ph.D. thesis, Massachusetts Institute of Technology, June 2005

[7] Ihler, A., Kernel Density Estimation Toolbox for MATLAB, http://www.ics.uci.edu/~ihler/code/kde.shtml

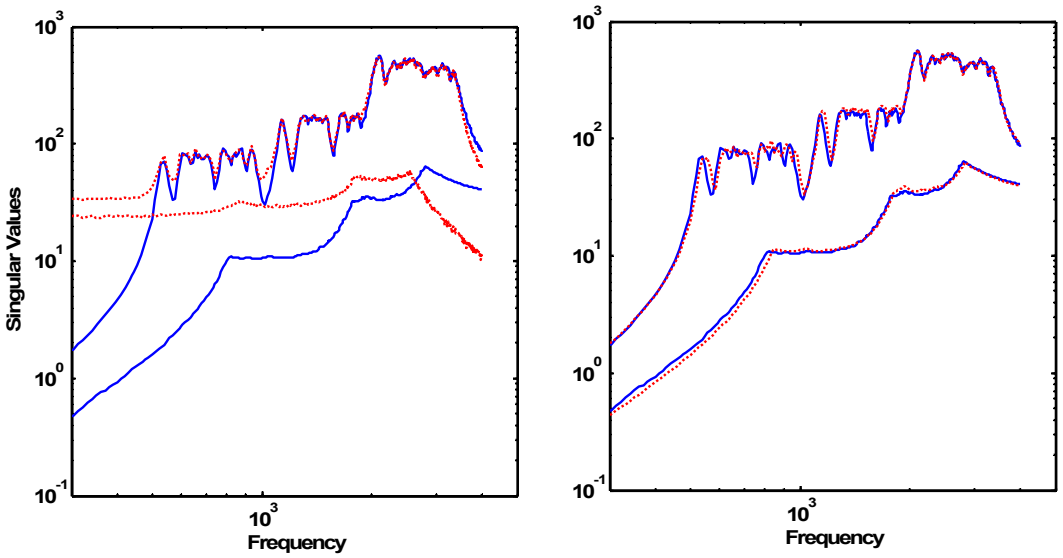

1a) Sandia original scripts 1b) Modified scripts

Fig. 1 Comparison of calibration data singular values bounds using the original Sandia script and revised script.

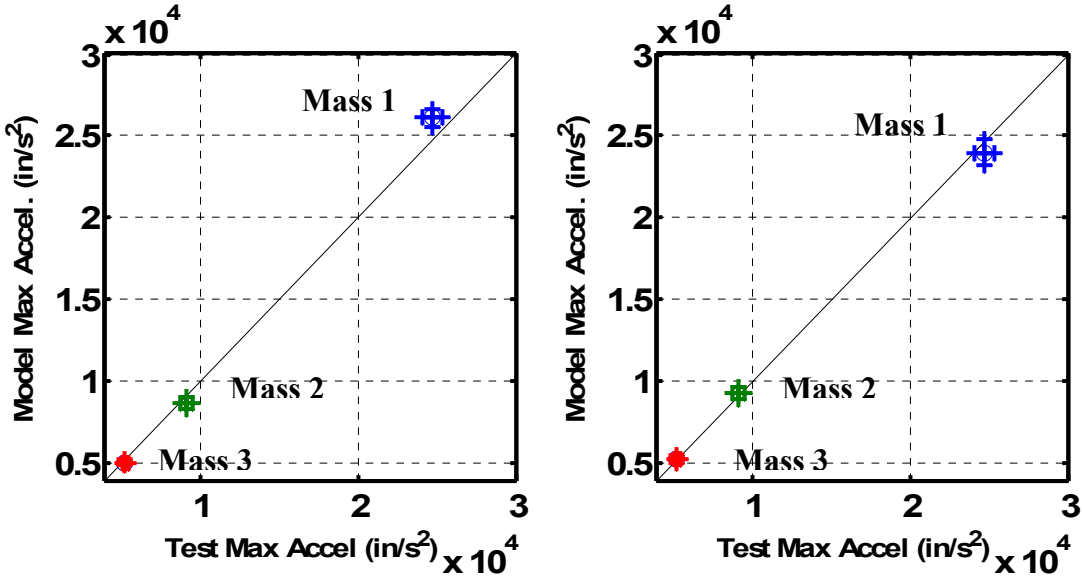

2a) Sandia original scripts 2b) Modified scripts

Fig. 2 Comparison of Metric 2 for the calibration data using original Sandia script and revised script.

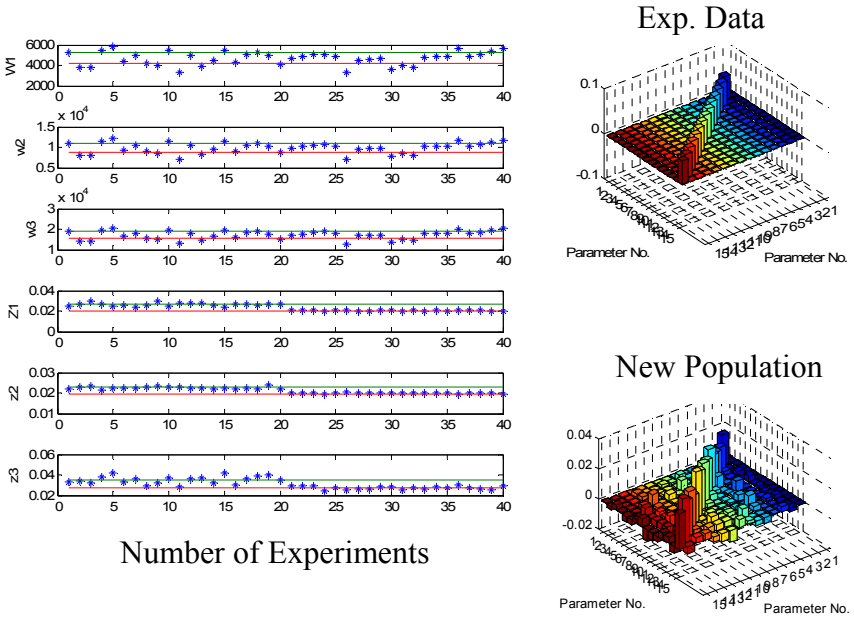

3a) Sample frequencies and damping 3b) Covariance

Fig. 3 PM-1 results with 99.9 % MLE CI Using Calibration and Validation Data

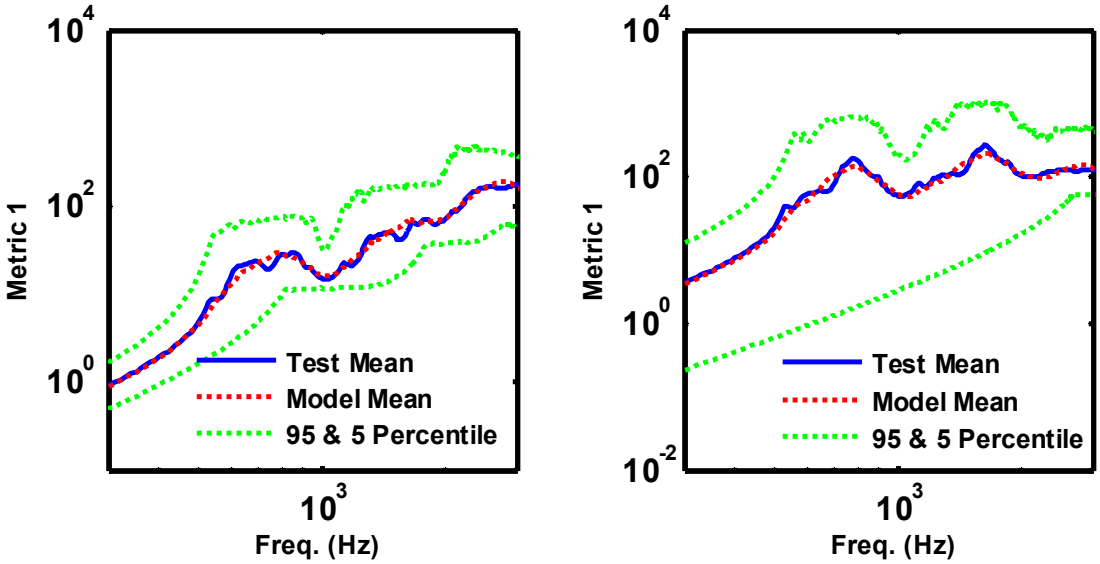

4a) Calibration Data 4b) Calibration and Validation Data

Fig. 4 PM-1 Comparison of Metric 1 (Population size 200)

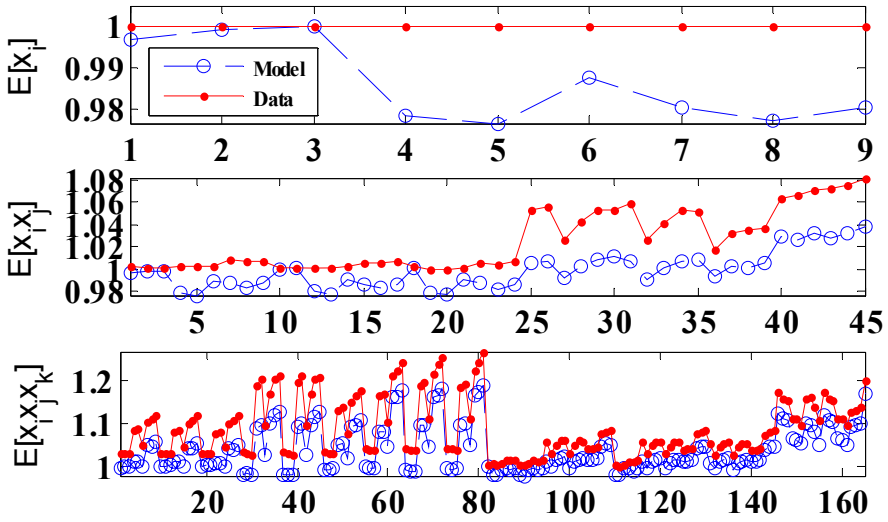

Fig. 5 1st, 2nd, and 3rd moment results from matching PM-2 parameters with Calibration data

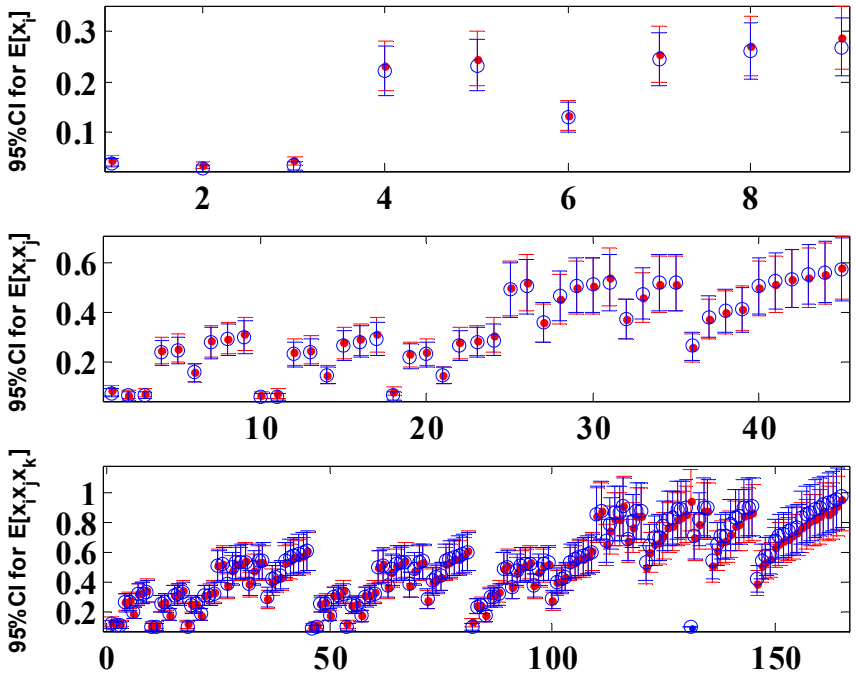

Fig. 6 Confidence intervals for the standard deviation of the results in figure 5

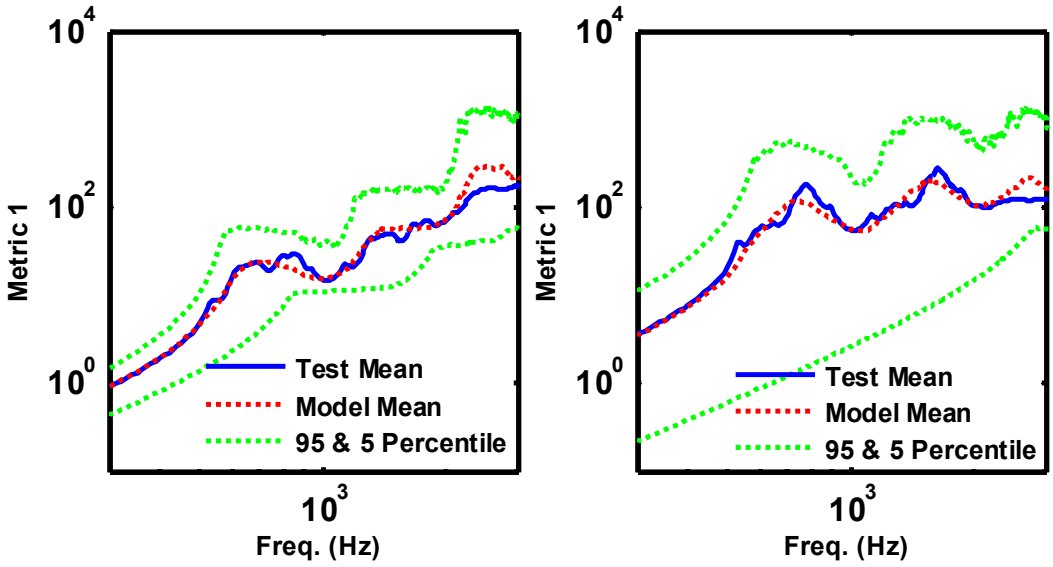

7a) Calibration Data 7b) Calibration & Validation

Fig. 7 PM-2 Comparison of Metric 1 (Population size 200)

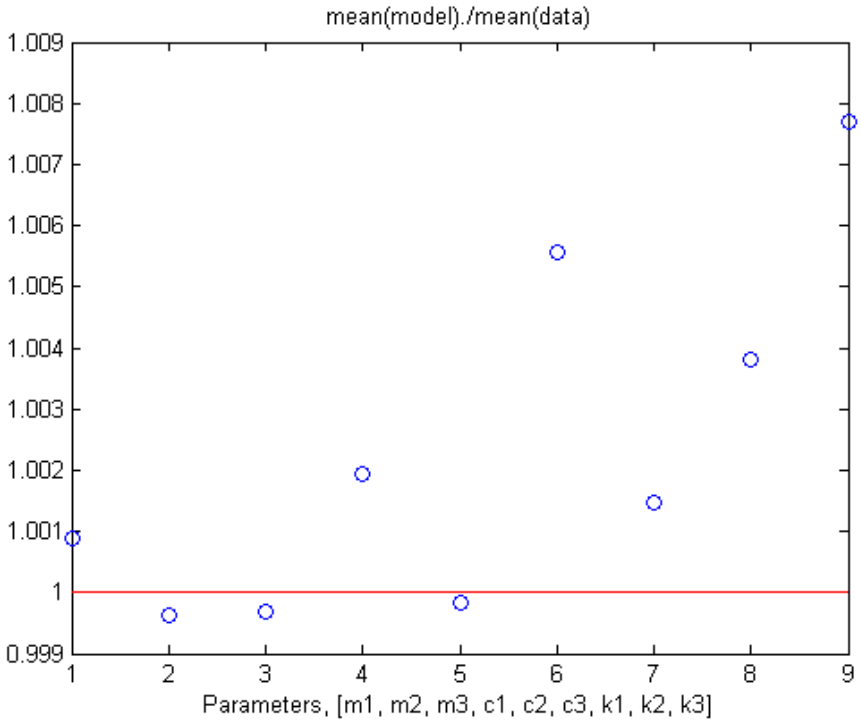

Fig. 8 Identified KDE parameters versus experimental data

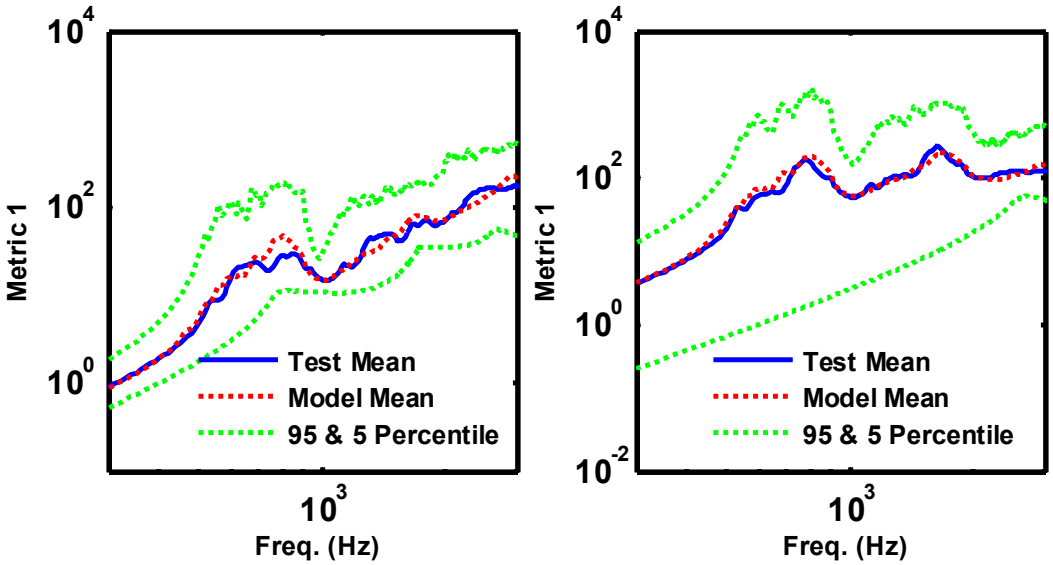

9a) Calibration Data 9b) Calibration & Validation

Fig. 9 PM-3 Comparison of Metric 1 (Population size 200)

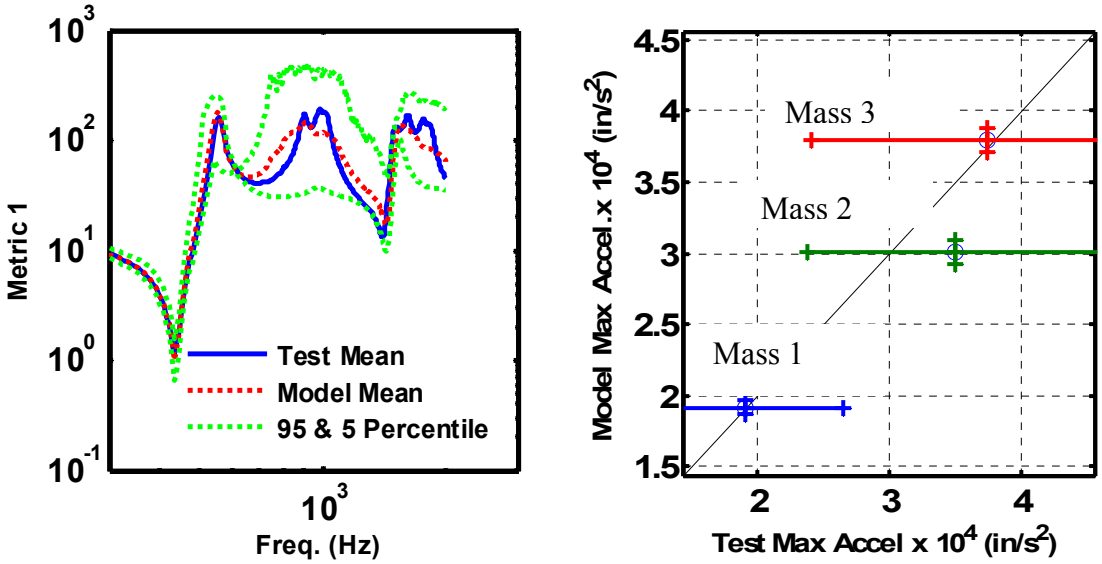

10a) Metric 1 10b) Mean and 95% CI for Metric 2

Fig. 10 Verification of Accreditation System Response Bounds PM-1 (Population Size 200)

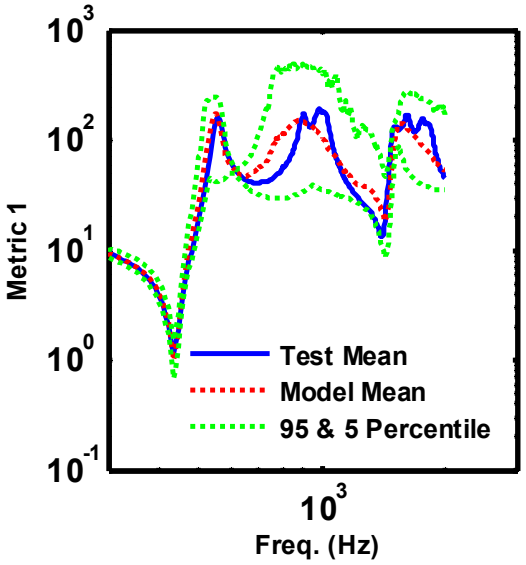

11a) Metric 1

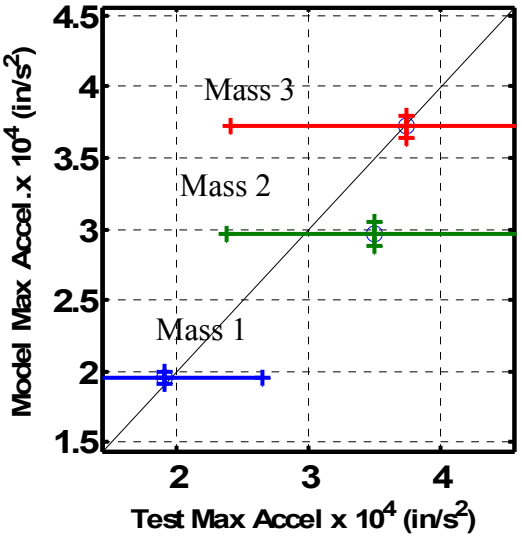

11b) Mean and 95% CI for Metric 2

Fig. 11Verification of accreditation system response bounds PM-2
(Population Size 200)

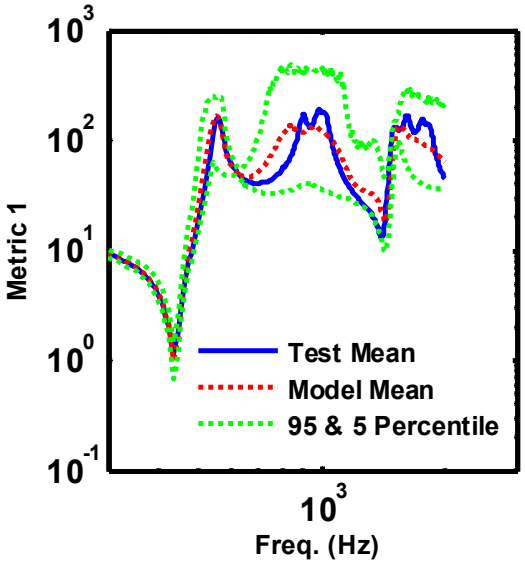

12a) Metric 1

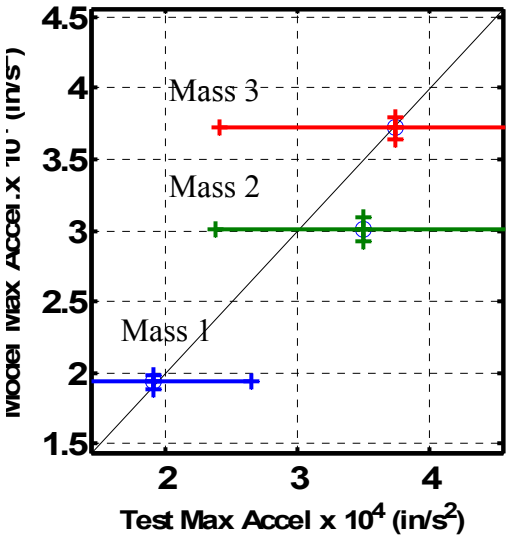

12b) Mean and 95% CI for Metric 2

Fig. 12 Verification of accreditation system response bounds PM-3
(Population Size 200)

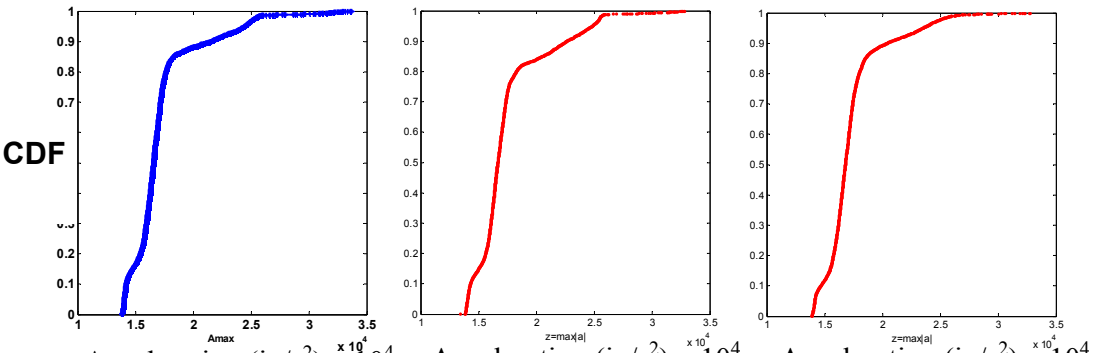

Acceleration (in/s^2) x 10^4 Acceleration (in/s^2) x 10^4 Acceleration (in/s^2) x 10^4

13a) PM-1, P_f=0.17 13b) PM-2, P_f=0.22 13c) PM-3, P_f=0.20

Fig. 13 Target System Mass 3 maximum acceleration CDF using Calibration Data (Population Size 5000)

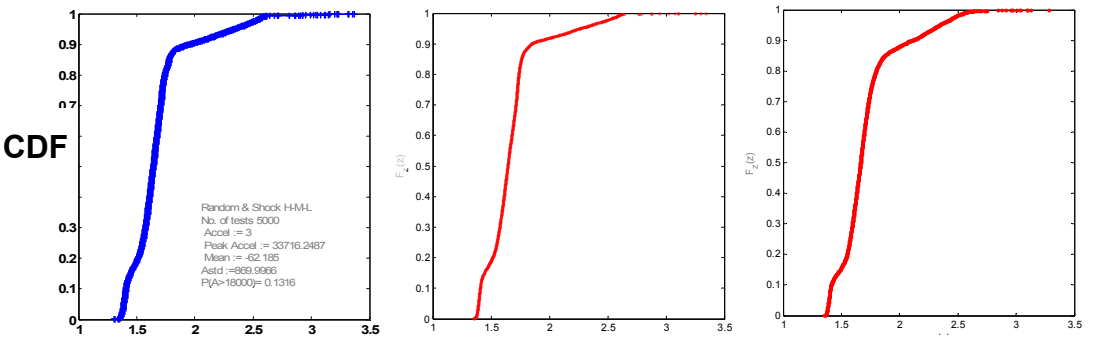

Acceleration (in/s^2) x 10^4 Acceleration (in/s^2) x 10^4 Acceleration (in/s^2) x 10^4

14a) PM-1, P_f=0.13 14b) PM-2, P_f=0.12 14c) PM-3, P_f=0.20

Fig. 14 Target System Mass 3 maximum acceleration CDF using Calibration and Validation Data (Population Size 5000)